Properties and Behavior of CTBN-Modified Epoxy with IPN Structure

Ying-Gev Hsu, Chin-Wei Liang

Department of Polymer Science and Engineering, National Taiwan University of Science and Technology, Taipei 106, Taiwan

Received 12 May 2006; accepted 13 August 2006
DOI 10.1002/app.25412
Published online 17 July 2007 in Wiley InterScience (www.interscience.wiley.com).

ABSTRACT: CTBN-modified epoxy resins (CMEs) with an interpenetrating-network (IPN) structure and a nanometer-sized morphology were prepared. Two systems of CMEs, called CNE/DDS/I-CTBN-B and CNE/DDS/I-CTBN-D, with IPN structures, were synthesized by heat-curing a homogeneous resin, CNE/DDS/CTBN/2-MI, obtained by mixing a carboxyl-terminated butadiene–acrylonitrile liquid rubber (CTBN) with a solution of polyglycidyl ether of *o*-cresol-formaldehyde novolac (CNE), 4,4′-diamino diphenyl sulfone (DDS), and 2-methyl imidazole (2-MI), in the presence of benzoyl peroxide and dicumyl peroxide, respectively. The IPN morphologies of the two systems of CMEs were identified by small-angle X-ray scattering by measuring the value of the specific interfacial surface area S_{sp} between the cured CNE/DDS matrix and the vulcanized CTBN. Properties such as fracture toughness, internal stress, and thermal and dynamic mechanical properties of these IPN-structured CMEs were studied in detail, and were compared with those of a conventional CME, CNE/DDS/CTBN, obtained by dispersing CTBN particles in a crosslinked CNE/DDS matrix. © 2007 Wiley Periodicals, Inc. J Appl Polym Sci 106: 1576–1584, 2007

Key words: CTBN-modified epoxy; interpenetrating network (IPN); small-angle X-ray scattering; nanometer-sized morphology

INTRODUCTION

Epoxy resins are thermoset polymers that exhibit good adhesion, high strength, and resistance to creep, heat, and chemicals. However, these polymers are brittle and exhibit poor toughness. Their toughness is often improved by introducing a dispersed rubber phase into the primary epoxy phase. These rubber-modified epoxy resins are prepared by heat-curing a homogeneous mixture of epoxy and a liquid rubber, such as carboxyl-terminated butadiene–acrylonitrile liquid rubber (CTBN).[1] It is well known that the cured resins are two-phase systems, in which the liquid rubber is dispersed in a matrix of epoxy with a spherical domain structure or a cocontinuous structure, as a result of phase separation, which proceeds via spinodal decomposition induced by the increase in molecular weight of the epoxy during the curing process.[2] However, the morphology and distribution of the CTBN in a phase-separated CTBN-modified epoxy resin (CME) is affected by the CTBN composition and the cure time and temperature.[3] It is, therefore, difficult to obtain a cocontinuous structure of the CME with a low CTBN content and high cure temperature, although the CME with cocontinuous structure exhibits excellent damping efficiency and high peel strength,[3] the CTBN, in most cases, is dispersed in a matrix of epoxy with a spherical domain structure.

In general, toughness improvement of CMEs is achieved when the CTBN particles are dispersed at the microscopic level, but it is always at the cost of a decrease in the modulus and the glass transition temperature (T_g) of the cured epoxy resin.[1,4] It is known that both the domain size (particle size) and the volume fraction of the rubber are critical factors which control the toughness of the cured epoxy resin.[5–7] To obtain the ultimate toughness while maintaining the valuable ductile behavior and minimizing the modulus loss of the cured epoxy resin, it would be preferable to introduce a nanosized (~30 nm) rubbery dispersion, subject to the condition of maintaining a critical interparticle distance with a smaller rubber volume fraction.[8] Since such a morphology cannot be prepared via conventional blending techniques, an alternative blending route has been explored, which involves chemically induced phase separation (CIPS) during the *in situ* polymerization, by a reaction of a reactive functional group such as carboxyl- and epoxide-containing rubber with the components (epoxy and amine) of the matrix.[8–10] The cured epoxy with a nanometer-sized rubbery phase is also obtained by interpenetrating between the epoxy/hardener and rubber networks.[11]

The effects of particle size on toughness of rubber-modified epoxies have been studied by many researchers. For example, Kim et al. [12] found that, for lower crosslinked diglycidyl ether of bisphenol A (DGEBA)/

Correspondence to: Y.-G. Hsu (yhsu@tx.ntust.edu.tw).
Contract grant sponsor: National Science Council of Taiwan.

TABLE I
Compositions of the CNE/DDS/CTBN/2-MI Resins

CTBN[a] content (wt %)	0	10	15	20	25	30
CNE[b]	7.698	6.921	6.532	6.143	5.754	5.365
DDS[b]	2.202	1.979	2.8575	1.757	1.646	1.535
CTBN	–	1.000	1.500	2.000	2.500	3.000
2-MI[c]	0.100	0.100	0.100	0.100	0.100	0.100
MEK	10.00	10.00	10.00	10.00	10.00	10.00

[a] CTBN (wt %) = CTBN/(CNE + DDS + 2MI + CTBN).
[b] Equivalent ratio of CNE to DDS = 1 : 1.
[c] 2-MI/(CNE + DDS + 2MI + CTBN) = 1 wt %.

piperidine resin, the fracture toughness of rubber-modified epoxies increases as the particle size of core–shell rubber decreases from 1.2 to 0.2 μm, because it obeys the cavitation (in rubber phase) and shear deformation (in matrix phase) toughness mechanisms. While fracture toughness is constant in this range of particle size for higher crosslinked DGEBA/diaminodiphenylmethane resin, it only obeys the cavitation (in rubber phase) toughness mechanism. However, toughening effectiveness decreases with <0.2 μm core shell rubber particles, since they are difficult to cavitate. Rebizant et al.[10] prepared rubber-modified epoxies with a domain size of 30–70 nm rubbery phase by incorporating the acid-containing block copolymer into the DGEBA/amines networks through CIPS process. The level of toughening for rubber-modified epoxies are 1.2–1.8-fold reinforced without sacrificing their T_g and dynamic mechanical properties significantly. Janson et al. [11] synthesized the full-IPN PMMA/epoxy blends with nanometer-sized morphology by simultaneous polymerization of the homogeneous solution of MMA and epoxy/amine monomers in the presence of an initiator, and were compared with the semi-IPN blends, obtained by dispersing epoxy/amine rubber phase in a thermoplastic PMMA matrix. They found that, for the full-IPN blend with nanometer-sized morphology, the microscopic deformation mechanism for the tensile deformation is transferred from crazing to complete shear yielding. Despite this, the macroscopic toughness is found to be rather system-independent, since for the two systems, a comparable synergistic toughening effect is observed in both tensile and impact deformation.

In the study described in this article, a new CME with an interpenetrating-network (IPN) structure and a nanometer-sized morphology was prepared by incorporating CTBN directly into an polyglycidyl ether of *o*-cresol-formaldehyde novolac/4,4′-diamino diphenyl sulfone (CNE/DDS) matrix (i.e., a solution of CNE and DDS), with a catalyst 2-methyl imidazole (2-MI), to form a homogeneous viscous resin. When this CNE/DDS/CTBN/2-MI resin is heated in the presence of a peroxide (e.g., benzoyl peroxide (BPO) or dicumyl peroxide (DCP)), the CNE/DDS and the CTBN undergo polyaddition and vulcanization, respectively, to afford a CME, CNE/DDS/I-CTBN, with an IPN structure. The morphology and properties, such as fracture toughness, internal stress, thermal stability, and dynamic mechanical properties, of this IPN-structured CME were studied and compared in detail with those of a conventional CME, CNE/DDS/CTBN, obtained by heat-curing the CNE/DDS/CTBN/2-MI resin (without any peroxide in the resin), where the CTBN particles were dispersed in a crosslinked CNE/DDS matrix.

EXPERIMENTAL

Materials

Polyglycidyl ether of *o*-cresol-formaldehyde novolac (CNE, CNE-200EL-F), with a weight per epoxy equivalent of 216 ± 2 g, was purchased from Chang-Chung Resin Co., Taiwan. CTBN (Hycar 1300 × 13, 26 wt % bound acrylonitrile, M_n = 3150) was supplied by Noveon Chemical, Hong Kong. DDS, 2-MI, BPO, and DCP were purchased from Acros Chemical (Geel, Belgium), and were used without further purification. Other reagents were purified by conventional methods.

Preparation of the CME

CMEs, of type CNE/DDS/CTBN and CNE/DDS/I-CTBN, were prepared as follows. Methyl ethyl ketone (MEK) solutions of CTBN, 2-MI, and peroxide (i.e., BPO or DCP) were added quantitatively to the CNE/DDS resin, separately, according to the procedures listed in Tables I and II. The mixtures were then stirred (for ~30 min) until homogeneity was attained. Transparent, viscous mixtures were obtained by removing MEK from the homogeneous solutions *in vacuo*. Films of transparent CMEs with a uniform thickness were prepared by heating the degassed viscous mixtures, which were cast onto a plate at 120°C for 2 h and then postcured at 160°C for 4 h, to induce an addi-

TABLE II
Content of Peroxide in the CNE/DDS/CTBN/2-MI Resins

BPO or DCP[a] content (wt %)	1	2	3	4	5
CNE[b]	6.128	6.112	6.096	6.081	6.065
DDS[b]	1.752	1.748	1.744	1.739	1.735
20 wt % CTBN[c]	2.000	2.000	2.000	2.000	2.000
2-MI[d]	0.100	0.100	0.100	0.100	0.100
BPO or DCP	0.020	0.040	0.060	0.080	0.100
MEK	10.00	10.00	10.00	10.00	10.00

[a] BPO or DCP = *x* wt % × CTBN.
[b] Equivalent ratio of CNE to DDS = 1 : 1.
[c] CTBN (wt %) = CTBN/(CNE + DDS + 2MI + CTBN).
[d] 2-MI/(CNE + DDS + 2MI+CTBN) =1 wt %.

tion reaction of the epoxide groups in the CNE, with the amino groups in the DDS in the presence of 2-MI and vulcanization of CTBN in the presence of peroxide.[13] Both polyaddition between CNE and DDS and vulcanization of CTBN are depicted in Scheme 1. The IPN-structured CMEs prepared by curing a CNE/DDS/CTBN/2-MI resin with a CTBN content of 20 wt % initiated by BPO are represented by ''CNE/DDS/I-CTBN-B'' in this article, and the CMEs initiated by DCP are represented by ''CNE/DDS/I-CTBN-D''.

Fracture toughness properties

The fracture toughness properties of the cured CNE/DDS matrix and the CMEs were characterized in terms of the critical stress intensity factor K_{IC} at fracture initiation, and were measured at 25°C using a TA Instruments DMAQ800 dynamic mechanical analyzer in accordance with ASTM D 5045-99.[14] A three-point bend flexural clamp with three identical cylindrical rollers was used to bend the sample, with a static force ranging from 1 to 18 N at a rate of 1 N/min. The three-point bend specimen was a single-edge-notched specimen, 20 mm in span, with a crack length a (crack prenotch plus razor notch) = B (width) = 2 mm, and 4 mm in thickness (D). K_{IC} was calculated from

$$K_{IC}(\text{MPa m}^{1/2}) = f(x)P_Q/(BD^{1/2}) \quad (1)$$

where $f(x) = 6x^{1/2}[1.99 - x(1 - x)(2.15 - 3.93x + 2.73x^2)]/(1 + 2x)(1 - x)^{3/2}$, $x = a/D$, and P_Q is the load at crack initiation.

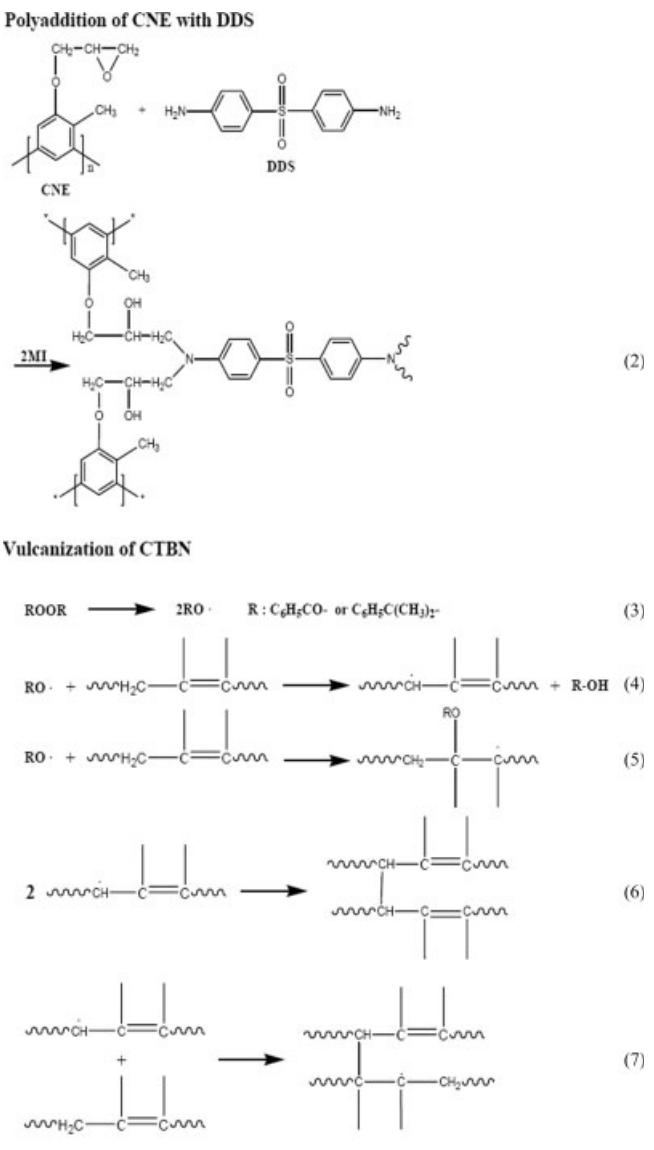

Scheme 1 Polyaddition between CNE and DDS and vulcanization of CTBN.

Thermal–mechanical analysis

The coefficients of thermal expansion of the cured CNE/DDS matrix and the CMEs were measured with a TA Instruments TMAQ400 thermal–mechanical analyzer, in accordance with ASTM E 831-86. The sample was heated at a heating rate of 10°C/min, under a N_2 flow of 50 cm^3/min. The thermal expansion increased with increasing temperature, and the coefficient of thermal expansion was calculated from the slope. An abrupt change in the slope of the expansion curve indicates a transition of the material from one state to another.

Flexural properties

The flexural properties of the cured CNE/DDS matrix and the CMEs were measured using a TA Instruments DMAQ800 dynamic mechanical analyzer.[14] A three-point bending clamp with three identical cylindrical rollers was used to bend the sample, with a static force ranging from 1 to 18 N at a rate of 1 N/min. A rectangular bar specimen with dimensions of $10 \times 5 \times 0.8$ mm^3 was chosen.

Morphology studies

Scanning electron microscopy (SEM) was used to observe the morphological features of the CMEs. The fractured surfaces of the specimens were coated with gold using a vacuum sputterer and examined using a S-3000N Hitachi (Japan) instrument. The domain formation process in the IPNs was measured with an Osmic (USA) PSAXS-USH-WAXS-002 small-angle-X-ray-scattering (SAXS) spectrometer. The X-ray source was operated at 45 kV and 0.67 mA. Cu Kα radiation ($\lambda = 0.154$ nm) was used.

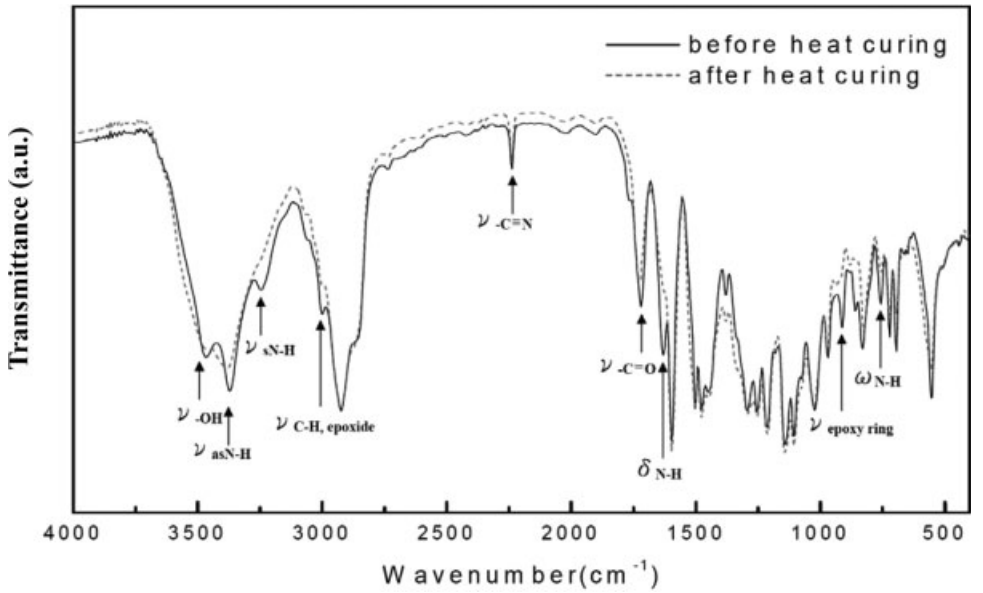

Figure 1 FTIR spectra of CNE/DDS/CTBN-20 (with CTBN content of 20 wt %) before and after heat treatment.

Measurement

Fourier transform infrared (FTIR) spectra of the samples were recorded on a Digilab FTS-1000 FTIR instrument with a resolution of 4 cm^{-1}. Samples for FTIR measurement were prepared by coating the polymer or homogeneous mixture onto a KBr disk, followed by vacuum drying (<5 Torr) at 40°C for 10 h. Differential scanning calorimetry (DSC) of the systems was performed using a TA Instruments DuPont Q1000 DSC at a heating rate of 10°C/min. The decomposition point (T_d) of the CMEs was determined using a TA Instruments DuPont Q500 thermogravimetric analyzer at a heating rate of 10°C/min, under a N_2 flow rate of 20 mL/min. The dynamic mechanic properties of the materials were measured using a TA Instruments DMAQ800 dynamic mechanical analyzer. The driving frequency was 1 Hz, with a heating rate of 5°C/min. A rectangular bar specimen with dimensions of 20 $\times$ 10 $\times$ 1 mm^3 was chosen.

RESULTS AND DISCUSSION

Preparation of CMEs

CNE/DDS/CTBN was prepared by heating a homogeneous solution of CNE, DDS, CTBN, and 2-MI (Table I). Figure 1 shows FTIR spectra of CNE/DDS/CTBN before and after heat-curing. The characteristic absorption peaks of CNE/DDS/CTBN before heat treatment at 3470 cm^{-1} (ν_{-OH}), 3370 and 3240 cm^{-1} (ν_{-NH}), 3060 cm^{-1} ($\nu_{C-H,\ epoxide}$), 1630 and 1515 cm^{-1} ($\delta_{-NH,\ DDS}$ and $\nu_{benzene\ ring,\ CNE}$), 910 cm^{-1} ($\nu_{epoxide\ ring}$), zand 770 cm^{-1} (ω_{-NH}) are shown (solid lines). After heat treatment at 160°C for 4 h, the absorption bands at 3370, 3240, 3060, 1630, 910, and 770 cm^{-1} disappear or decrease significantly in intensity (dashed lines) because of the reaction between epoxide groups in the CNE and amino groups in the DDS (Scheme 1). It is difficult to measure whether the terminated carboxylic group in the CTBN reacts with epoxide or amino groups in the CNE/DDS matrix by investigating the

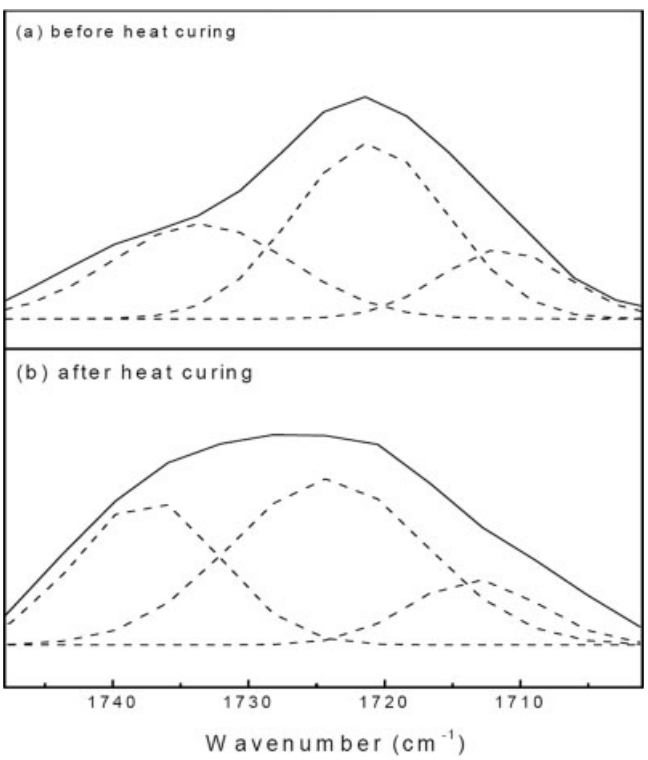

Figure 2 FTIR spectra of carbonyl absorption of cured CNE/DDS/CTBN-20 and the corresponding Gaussian fitted peaks.

TABLE III
Peak Areas of Carbonyl Absorption for the CTBN in CNE/DDS/CTBN Before and After Heat-Curing

Wave number (cm^{-1})	Peak area ratios[a]		Percentage of peak areas (%)	
	Before	After	Before	After
1736	2.4764 (1.2754)[b]	1.7638 (1.8710)	37.23 (40.37)	38.62 (58.81)
1724	3.0770 (1.4042)	2.0574 (1.2543)	46.26 (44.45)	45.05 (39.42)
1713	1.0979 (0.4793)	0.7456 (1.7850)	16.51 (15.13)	16.33 (1.77)

[a] Peak areas of carbonyl group absorptions were obtained through Gaussian peak fitting method and were calibrated by the peak area of —CN group.
[b] Values in parentheses were peak areas of carbonyl absorptions for the recipe not catalyzed by 2-MI.

shift of the carbonyl absorption in the FTIR spectrum. However, through a Gaussian peak-fitting method (Fig. 2),[15] it was found that, in the presence of 2-MI, the peak areas (calibrated by the area of —CN absorption) of carbonyl absorption at 1737, 1724, and 1713 cm^{-1} before and after heat treatment were only a little different from each other when compared with those obtained using a recipe without the 2-MI catalyst (Table III). This phenomenon suggests that the reaction between CTBN and the CNE/DDS matrix in the presence of 2-MI occurs only to a very limited extent, and perhaps can be neglected. Figure 3 displays DSC traces of CTBN in the presence of 1 wt % of BPO and DCP, respectively, at a heating rate of 10°C/min over the temperature region 40–180°C. The existence of exothermic peaks in the DSC curves A and B indicates that both BPO and DCP initiate the exothermic vulcanization of CTBN. In contrast, when the CNE/CTBN mixture was studied using the same heating conditions, there was no thermal peak to show any reaction between CNE and CTBN (curve C). Therefore, when the CNE/DDS/CTBN/2-MI resin is heated in the presence of both peroxide and 2-MI, an IPN-structured CME, CNE/DDS/I-CTBN, is obtained by a CIPS procedure involving two crosslinking reactions—polyaddition between CNE and DDS [eq. (2)] and vulcanization of CTBN [eqs. (3)–(7)].

Morphologies of the CMEs

Figure 4 shows SEM images of the conventional CNE/DDS/CTBN and the IPN-structured CNE/DDS/I-CTBN. Figure 4(a) and (b) shows the morphologies of CNE/DDS/CTBN-10 and CNE/DDS/CTBN-20 (''CTBN-10'' denotes a CME containing 10 wt % of CTBN in the CME, and ''CTBN-20'' denotes a CME containing 20 wt % of CTBN). Fine uniform globules, about a micrometer in diameter, are seen. The CTBN is thought to coarsen during polymerization and phase separation at high temperature.[11] Figure 4(c) and (d) shows the morphologies of CNE/DDS/I-CTBN-1B and CNE/DDS/I-CTBN-1D (''-1B'' denotes a CME containing 20 wt % of CTBN, heat-cured in the presence of BPO, with a content of BPO relative to CTBN of 1 wt %; ''-1D'' denotes a similar CME with a content of DCP of 1 wt % (Table II)). The morphologies of the CNE/DDS/I-CTBN samples are very smooth and are quite different from those of the conventional CNE/DDS/CTBN. It can be presumed that the vulcanized CTBN interpenetrates the CNE/DDS matrix on a nanometer scale, which suppresses the coarsening process during polymerization and phase separation.

Analysis of the IPN morphology of CNE/DDS/I-CTBN CMEs

The SAXS technique has proved to be applicable to the analysis of IPN morphologies, in spite of the ambiguity in the physical meaning of the correlation function.[16–18] Figure 5 shows Debye–Bueche plots displayed in terms of $I^{-1/2}$ (where I is the scattering intensity) versus S^2 (where S is the scattering vector in reciprocal space) for CNE/DDS/CTBN-20, CNE/DDS/I-CTBN-3B, and CNE/DDS/I-CTBN-3D (''-3B'' denotes a CME containing 20 wt % of CTBN, heat-cured in the presence of BPO, with a content of BPO relative to CTBN of 3 wt %; ''-3D'' denotes a similar

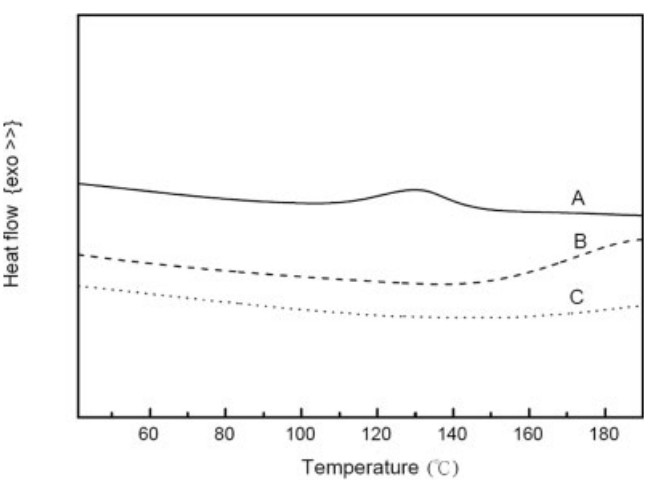

Figure 3 DSC traces of CTBN in the presence of 1 wt % of (A) BPO and (B) DCP, and (C) DSC trace of CNE/CTBN (w/w: 60/40), at a heating rate of 10°C/min over the temperature range 40–180°C.

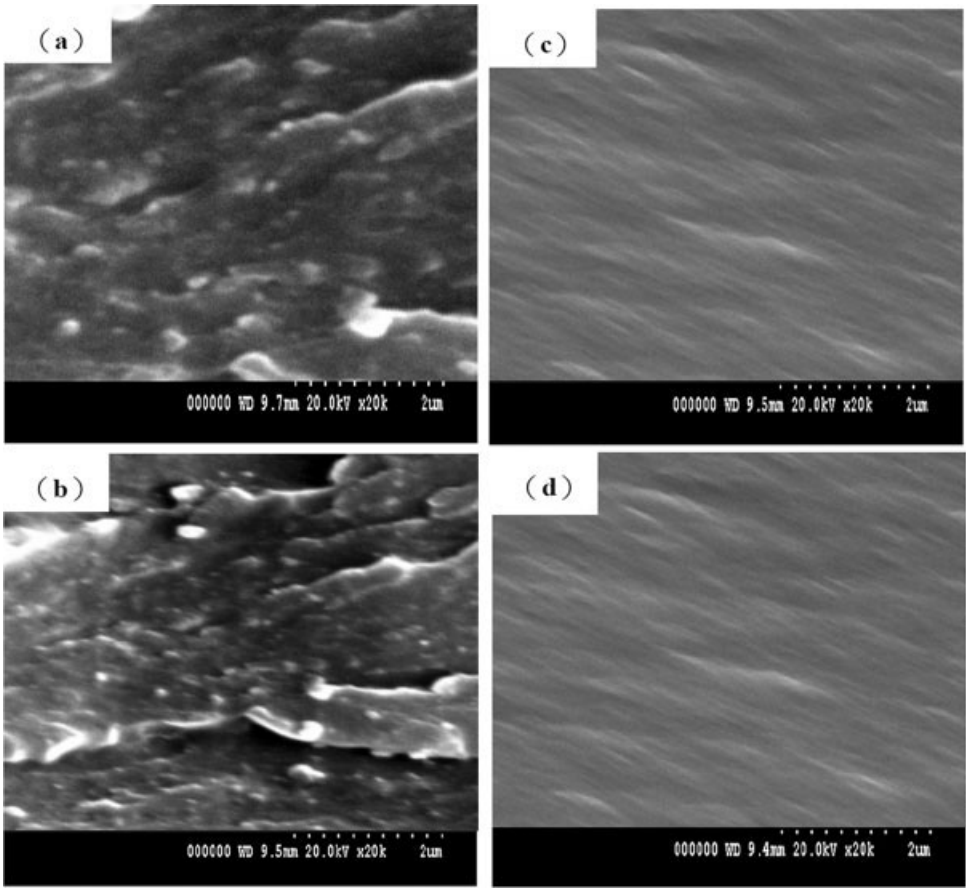

Figure 4 SEM images of (a) CNE/DDS/CTBN-10, (b) CNE/DDS/CTBN-20, (c) CNE/DDS/I-CTBN-1B, and (d) CNE/DDS/I-CTBN-1D.

CME with a content of DCP of 3 wt % (Table II)). Straight lines were drawn and the short-range correlation distance a_1, which is used to measure the intraparticle distance, was determined from the sum of the slope and the intercept of the linear portion.[17,18]

Figure 6 is a Guinier plot in terms of ln I versus S^2 for CNE/DDS/CTBN-20, CNE/DDS/I-CTBN-3B, and CNE/DDS/I-CTBN-3D. The correlation distance a_2, which is used to measure the interparticle distance, was determined from the slope. Phase dimensions determined

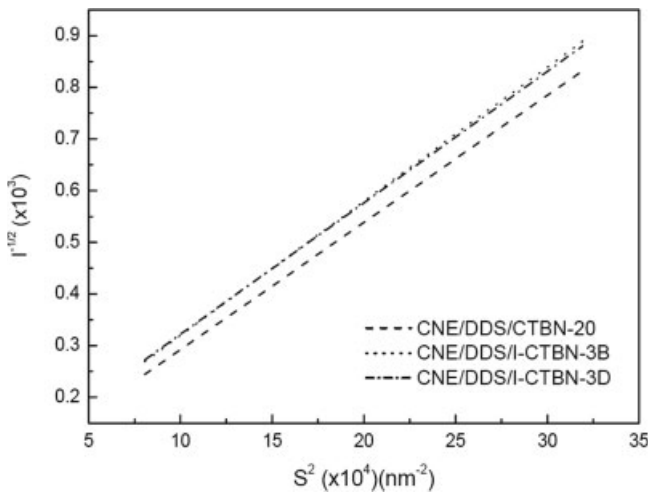

Figure 5 Debye–Bueche plots of $I^{-1/2}$ versus S^2 for CNE/DDS/CTBN-20, CNE/DDS/I-CTBN-3B, and CNE/DDS/I-CTBN-3D.

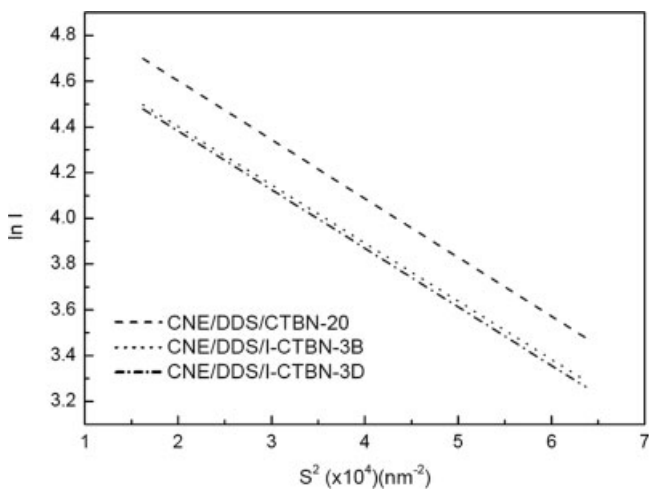

Figure 6 Guinier plots of ln I versus S^2 for CNE/DDS/CTBN-20, CNE/DDS/I-CTBN-3B, and CNE/DDS/I-CTBN-3D.

TABLE IV
Correlation Parameters of the Morphology of CMEs in the CNE/DDS/I-CTBN-B and CNE/DDS/I-CTBN-D Systems

	Correlation distance (Å)		
	a_1	a_2	S_{sp} (m^2/g)
CNE/DDS/CTBN-20	116.94	286.14	547.29
CNE/DDS/I-CTBN-1B	110.27	300.39	580.39
CNE/DDS/I-CTBN-2B	105.67	290.28	605.66
CNE/DDS/I-CTBN-3B	104.83	284.46	610.51
CNE/DDS/I-CTBN-4B	107.89	285.14	593.20
CNE/DDS/I-CTBN-5B	108.64	294.27	589.10
CNE/DDS/I-CTBN-1D	111.41	290.26	578.75
CNE/DDS/I-CTBN-2D	108.22	298.81	591.39
CNE/DDS/I-CTBN-3D	97.68	285.63	655.20
CNE/DDS/I-CTBN-4D	91.42	286.88	700.07
CNE/DDS/I-CTBN-5D	90.38	283.87	708.12

from the values of a_1 and a_2 are listed in Table IV. The specific interfacial surface area S_{sp}, which is used to measure the interpenetration between the components in the polymer networks, was determined, and is also listed in the table. The higher the value of S_{sp} the more extensive the interpenetration between the polymer networks.

The experimental results show that the values of S_{sp} for the CMEs in the CNE/DDS/I-CTBN-B and CNE/DDS/I-CTBN-D systems were higher than those for the conventional CNE/DDS/CTBN-20. The results also confirm the presumption made earlier that, when a CNE/DDS/CTBN/2-MI solution is heat-cured in the presence of BPO or DCP, the CTBN vulcanizes and interpenetrates with the cured CNE/DDS matrix on a nanometer scale, to form a CME with an IPN structure. However, all S_{sp} values for the CMEs in the CNE/DDS/I-CTBN-B system, with various contents of BPO, are lower than for the CMEs in the CNE/DDS/I-CTBN-D system with corresponding contents of DCP. This phenomenon can be presumed as that BPO (E_a = 111.3 kJ/mol)[19] is more reactive than DCP (E_a = 125.4 kJ/mol).[20] The BPO starts to initiate the vulcanization of the CTBN at a lower temperature than does DCP (BPO can even start the reaction at room temperature). Thus, at the same curing temperature (e.g., 120°C), a CNE/DDS/CTBN/2-MI resin initiated by BPO is more viscous than a similar resin initiated by DCP, and this BPO-initiated resin is more difficult for the interpenetration between the CTBN network and CNE/DDS matrix than the resin initiated by DCP.[21] The S_{sp} values for the CMEs in both the CNE/DDS/I-CTBN-B and the CNE/DDS/I-CTBN-D systems increase with the content of BPO or DCP.

Toughening of CMEs

The fracture toughness of the CNE/DDS/CTBN and IPN-structured CNE/DDS/I-CTBN CMEs was evaluated from the critical value of the stress intensity factor K_{IC} for the initiation of crack growth, which was determined from the three-point bend specimens according to ASTM D 5045-99.[22,23] Figure 7 shows the variation of K_{IC} for CNE/DDS/CTBN with increasing CTBN content. The fracture toughness increases with the content of CTBN (increases are observed from 0 to 10 wt %, from 10 to 15 wt %, and from 15 to 20 wt %), until a maximum is reached at 20 wt % CTBN; further increase in the content results in a slightly decreased fracture toughness. The content of CTBN of 20 wt % in the CME seems to be the optimum condition. Therefore, in the rest of this study, the content of CTBN in both the CNE/DDS/I-CTBN-B and the CNE/DDS/I-CTBN-D system was kept constant at 20 wt %, and we compared their toughness, internal stress, dynamic mechanical properties, and gravimetric properties with those of the corresponding CNE/DDS/CTBN-20. Table V lists the K_{IC} values of the CMEs in the CNE/DDS/I-CTBN-B and CNE/DDS/I-CTBN-D systems. It was found that the K_{IC} values of the CMEs in both systems, for various peroxide/CTBN ratios, were all higher than those of CNE/DDS/CTBN-20 and the CNE/DDS matrix. The experimental results suggest that the fracture toughness of CMEs with an IPN structure is superior to that of conventional CNE/DDS/CTBN.

Internal stress in CMEs

The internal stress in a CME is closely related to the product of the flexural modulus and the thermal expansion coefficient below the glass transition temperature of the cured resin.[24] Therefore, it is necessary to reduce the coefficient of thermal expansion α_1 and/or the flexural modulus E_r of the CME, to reduce the internal stress S. Figure 8 shows the internal

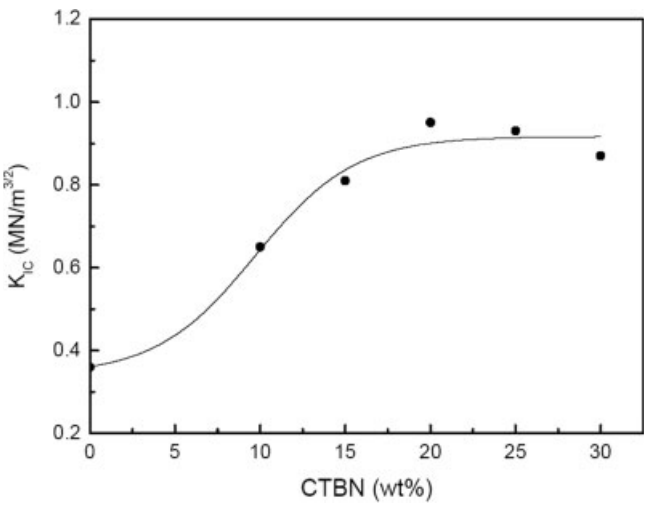

Figure 7 Variation of K_{IC} for CNE/DDS/CTBN with increase of CTBN content.

TABLE V
K_{IC} for CMEs in the CNE/DDS/I-CTBN-B and CNE/DDS/I-CTBN-D Systems with Various Contents of Peroxide

	K_{IC}[a] ($MN/m^{3/2}$)				
Peroxide (wt %)	1.0	2.0	3.0	4.0	5.0
CNE/DDS/I-CTBN-B[c]	1.07 ± 0.04	1.07 ± 0.08	1.30 ± 0.09	1.01 ± 0.01	0.96 ± 0.08
CNE/DDS/I-CTBN-D[d]	0.96 ± 0.08	1.10 ± 0.14	1.13 ± 0.03	0.95 ± 0.08	0.97 ± 0.07

[a] For K_{IC} CNE/DDS matrix and CNE/DDS/CTBN-20 were 0.36 and 0.95 $MN/m^{3/2}$, respectively.
[b] wt % = (BPO or DCP/CTBN) × 100.
[c] CNE/DDS/CTBN-20 was heat-cured in the presence of BPO.
[d] CNE/DDS/CTBN-20 was heat-cured in the presence of DCP.

stresses of CMEs in the CNE/DDS/I-CTBN-B and CNE/DDS/I-CTBN-D systems at various peroxide/CTBN ratios. It was found that the internal stresses for the CNE/DDS/I-CTBN-B and CNE/DDS/I-CTBN-D systems were all lower than those for the CNE/DDS matrix and CNE/DDS/CTBN-20. The experimental results show that CNE/DDS/I-CTBN with an IPN structure has not only a higher fracture toughness, but also a reduced internal stress to a significant degree, at an optimum peroxide/CTBN ratio. This can be attributed to the complete separation (but with entangling) of the vulcanized CTBN phase from the CNE/DDS matrix, the vulcanized CTBN acting as a stress-relieving phase.[25]

Thermal stability of CMEs

Figure 9 shows the thermogravimetric analysis (TGA) curves of the CNE/DDS matrix, CNE/DDS/CTBN-20, CNE/DDS/I-CTBN-3B, and CNE/DDS/I-CTBN-3D. It was found that both of the IPN-structured materials, CNE/DDS/I-CTBN-3B and CNE/DDS/I-CTBN-3D, had a higher decomposition temperature (T_d) than the corresponding CNE/DDS/CTBN-20 and the CNE/DDS matrix. The higher T_d of CNE/DDS/I-CTBN-3B and CNE/DDS/I-CTBN-3D is due to the interpenetration of the vulcanized CTBN and the CNE/DDS matrix.

Dynamic mechanical properties of CMEs

The dynamic mechanical properties of the CNE/DDS matrix, and of the conventional and IPN-structured CMEs were studied.[25,26] Figure 10 shows plots of the storage modulus E' and tan δ versus temperature for the CNE/DDS matrix, CNE/DDS/CTBN-20, CNE/DDS/I-CTBN-3B, and CNE/DDS/I-CTBN-3D. Two distinct transition peaks in the tan δ curves are found for both CNE/DDS/I-CTBN-3B and CNE/DDS/I-CTBN-3D; this result is similar to that for CNE/DDS/CTBN-20, indicating that phase separation has occurred in these materials. In contrast, only one, rel-

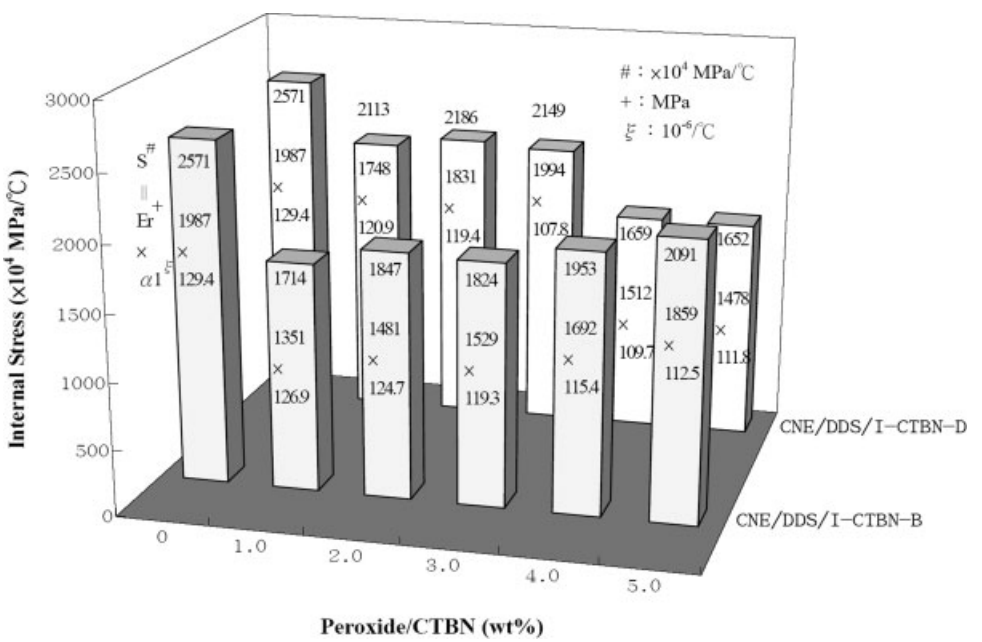

Figure 8 Internal stresses of CMEs in the CNE/DDS/I-CTBN-B and CNE/DDS/I-CTBN-D systems for various peroxide/CTBN ratios.

atively narrow transition is found for the CNE/DDS matrix. The T_g values for the vulcanized CTBN in the two systems are a little higher than for the CTBN in CNE/DDS/CTBN-20. The tan δ peaks for CNE/DDS/I-CTBN-3B and CNE/DDS/I-CTBN-3D decrease in height and increase in breadth, revealing that the motion of the CNE/DDS matrix is restricted by the vulcanized CTBN because of extensive interpenetration of the two components. The major T_g values for these IPN-structured CMEs are equal to or only slightly lower than the values for the CNE/DDS matrix and the conventional CNE/DDS/CTBN-20. Although the storage moduli for the two systems are lower than that of the CNE/DDS matrix, they are still higher than that of the conventional CNE/DDS/CTBN-20.

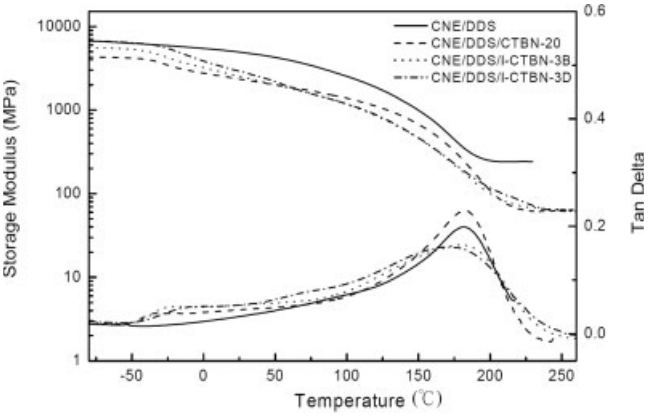

Figure 10 Plots of storage modulus (E') and tan δ versus temperature for CNE/DDS matrix, CNE/DDS/CTBN-20, CNE/DDS/I-CTBN-3B, and CNE/DDS/I-CTBN-3B

CONCLUSIONS

Two systems of IPN-structured CMEs, namely CNE/DDS/I-CTBN-B and CNE/DDS/I-CTBN-D, with a nanometer-sized morphology, have been prepared by heat-curing of CNE/DDS/CTBN/2-MI resins in the presence of BPO or DCP of different decomposition E_a. The IPN morphologies of the CMEs in the two systems, with various contents of peroxide, were confirmed by the fact that the materials had much higher S_{sp} values, measured by the SAXS technique, than those of conventional CNE/DDS/CTBN materials of corresponding CTBN content. The IPN-structured CMEs not only had higher fracture toughness and thermal stability, but also had a lower internal stress than the cured CNE/DDS matrix and conventional CNE/DDS/CTBN, without sacrificing their T_g and dynamic mechanical properties significantly. It was found that although the CMEs in the CNE/DDS/I-CTBN-B and CNE/DDS/I-CTBN-D systems had different degrees of interpenetration, the properties of the materials did not differ to a significant extent.

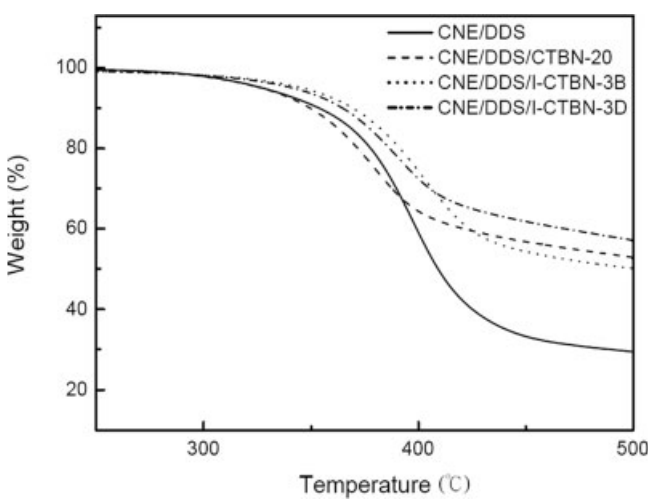

Figure 9 TGA curves of CNE/DDS matrix, CNE/DDS/CTBN-20, CNE/DDS/I-CTBN-3B, and CNE/DDS/I-CTBN-3D.

References

1. Pearson, R. A.; Yee, A. F. J Mater Sci 1986, 21, 2475.
2. Yamanaka, K.; Inoue, T. J Mater Sci 1990, 25, 241.
3. Yamanaka, K.; Takagi, Y.; Inoue, T. Polymer 1989, 60, 1839.
4. Kinloch, A. J.; Huang, Y. J Mater Sci 1992, 27, 2763.
5. Sultan, J. N.; Mcgarry, F. Polym Eng Sci 1973, 13, 29.
6. Russell, B.; Chartoff, R. Polymer 2005, 46, 785.
7. Azimi, H. R.; Pearson, R. A.; Hertzberg, R. W. J Mater Sci 1996, 31, 3777.
8. Jansen, B. J. P.; Rastogi, S.; Meijer, H. E. H.; Lemstra, P. J. Macromolecule 2001, 34, 3998.
9. Grubbs, R. B.; Dean, J. M.; Bates, F. S. Macromolecules 2001, 34, 8593.
10. Rebizant, V.; Venet, A. S.; Tournilhac, F.; Girard-Reydet, E.; Navarro, C.; Pascault, J. P.; Leibler, L. Macromolecules 2004, 37, 8017.
11. Jansen, B. J. P.; Rastogi, S.; Meijer, H. E. H.; Lemstra, P. J. Macromolecules 1999, 32, 6290.
12. Kim, D. S.; Cho, K.; Kim, J. K.; Park, C. E. Polym Eng Sci 1996, 36, 767.
13. Eirich, F. R. Science and Technology of Rubber; Academic Press: New York, 1978; Chapter 7.
14. Lee-Sullivan, P.; Dykeman, D. Polym Test 2000, 19, 239.
15. Seco, A. M.; Goncalves, M. C.; Almeida, R. M. Mater Sci Eng B 2000, 76, 193.
16. An, J. H.; Fernandez, A. M.; Sperling, L. H. Macromolecules 1987, 20, 191.
17. Tan, S. S.; Zhang, D. H.; Zhou, E. L. Polym Int 1997, 42, 90.
18. Yu, X. Q.; Gao, G.; Wang, J. Y.; Li, F.; Tang, X. Y. Polym Int 1999, 48, 805.
19. Hou, H. Y.; Shu, C. M. J Therm Anal Calorim 2006, 83, 41.
20. Dixon, K. W. In Polymer Handbook, 4th ed.; Brandrup, J., Immergut, E. H., Grulke, E. A., Eds.; Wiley: New York, 1999; Chapter II, p 29.
21. Mimura, K.; Ito, H.; Fujioka, H. Polymer 2000, 41, 4451.
22. Teng, K. C.; Chang, F. C. Polymer 1996, 37, 2385.
23. Ochi, M.; Shimaoka, S. Polymer 1999, 40, 1305.
24. Lin, L. L.; Ho, T. H.; Wang, C. S. Polymer 1997, 38, 1997.
25. Ho, T. H.; Wang, C. S. Polymer 1996, 37, 2733.
26. Laskar, S.; Vidal, F.; Fichet, O.; Gauthier, C.; Teyssié, D. Polymer 2004, 45, 5047.